Solution-processed organic tandem solar cells with embedded optical spacers

Hadipour, Afshin; de Boer, Bert; Blom, Paul W. M.

Published in:
Journal of Applied Physics

DOI:
10.1063/1.2786024

Publication date:
2007

Solution-processed organic tandem solar cells with embedded optical spacers

Afshin Hadipour, Bert de Boer,[a] and Paul W. M. Blom
Molecular Electronics, Zernike Institute for Advanced Materials, University of Groningen, Nijenborgh 4, NL-9747 AG Groningen, The Netherlands

(Received 10 May 2007; accepted 8 August 2007; published online 4 October 2007)

We demonstrate a solution-processed polymer tandem solar cell in which the two photoactive single cells are separated by an optical spacer. The use of an optical spacer allows for an independent optimization of both the electronic and optical properties of the tandem cell. The optical transmission window of the bottom cell is optimized to match the optical absorption of the top cell by varying the layer thickness of the optical spacer. The two bulk heterojunction subcells have complementary absorption maxima at $\lambda_{max} \sim 850$ nm for the top cell and $\lambda_{max} \sim 550$ nm for the bottom cell. The subcells are electronically coupled in series or in parallel using four electrical contacts. The series configuration leads to an open-circuit voltage of >1 V, which is equal to the sum of both subcells. The parallel configuration leads to a high short-circuit current of 92 A/m^2, which is equal to the sum of both subcells. The parallel configuration results in a much higher efficiency compared to the series configuration. © *2007 American Institute of Physics*.
[DOI: 10.1063/1.2786024]

I. INTRODUCTION

To improve the absorption of the solar radiation by organic solar cells, materials with a broad absorption band have to be designed and produced or different narrow band absorbers have to be stacked or mixed in multiple junctions. Illumination of an organic semiconductor leads to the creation of electron-hole pairs (excitons) with a binding energy of 0.4 eV (Refs. 1–3) instead of free charges. The most common solution-processable organic solar cells today consist of an intimate mixture of donors (a conjugated polymer) and acceptors (a soluble fullerene derivative) throughout the whole active layer, which is called a bulk heterojunction (BHJ) structure.[4–6] The resulting bound electron-hole pair is subsequently separated,[7,8] and the electrons and holes are transported through the acceptor and donor phases, respectively, assisted by a driving force that is given by the potential difference between the cathode and the anode. Because of the narrow absorption properties of most commonly used donor materials such as the conjugated polymers poly(2-methoxy-5-(3′,7′- dimethyloctyloxy)-*p*-phenylenevinylene) (MDMO-PPV) and poly(3-hexylthiophene) (P3HT), a solar cell based on one single active layer is not able to efficiently absorb the complete solar flux.[9,10] In contrast to a single layer cell, a tandem structure using two donor materials with nonoverlapping absorption bands can cover a large part of the visible range of the solar spectrum.[11–18]

Recently, we reported a solution-processed organic tandem solar cell that was fabricated from conjugated polymers with complementary absorption spectra and separated by a conducting composite middle contact [Fig. 1(a)].[18] In this tandem cell, high energy photons are absorbed in the bottom cell and low energy photons are absorbed in the top cell. In such a stacked geometry, the middle electrode serves two different purposes, as a charge recombination center and as a protecting layer for the bottom cell during spin coating of the top cell. The subcells are electronically coupled together in series, which results in an open-circuit voltage (V_{OC}) of the tandem cell that equals the sum of the V_{OC} of each subcell. The layer thickness of the bottom cell had to be optimized to in such a way that the optical output coupling is adapted to the absorption of the top cell. A disadvantage of this approach is that the optimum thickness of the bottom cell, required to match the optical output, is not necessarily equal to the thickness where the bottom cell reaches its optimum performance. If, for example, a thickness of 300 nm is required for optical out coupling, the occurrence of unbalanced transport may lead to the formation of space charges, giving rise to a reduced fill factor (FF) and performance.[19–23] In order to improve the first generation solution-processed tandem cells, we introduce here an additional solution-processable, transparent, and insulating layer which serves as an optical spacer and leads to the fabrication of a four-contact tandem cell [Fig. 1(b)]. In this second generation tandem cell, the thickness of the bottom cell is optimized for its electrical performance and the optical output coupling is tuned by varying the thickness of the optical spacer on top of the bottom cell. The transmitted light through the complete stack (bottom solar cell with optical spacer) is matched with absorption spectrum of the top cell. Since the optical spacer is an insulator, the fabrication of tandem cells with four electrodes is feasible and, consequently, the two subcells can be coupled electronically (external) in parallel or in series.

II. EXPERIMENT

The devices were fabricated on cleaned glass/indium tin oxide (ITO) substrates. A 50 nm thick poly(ethylenedioxythiophene) poly(stryrenesulfonic acid) (PEDOT:PSS) (H. C.

[a]Author to whom correspondence should be addressed. FAX: +31 503638751. Electronic mail: b.de.boer@rug.nl

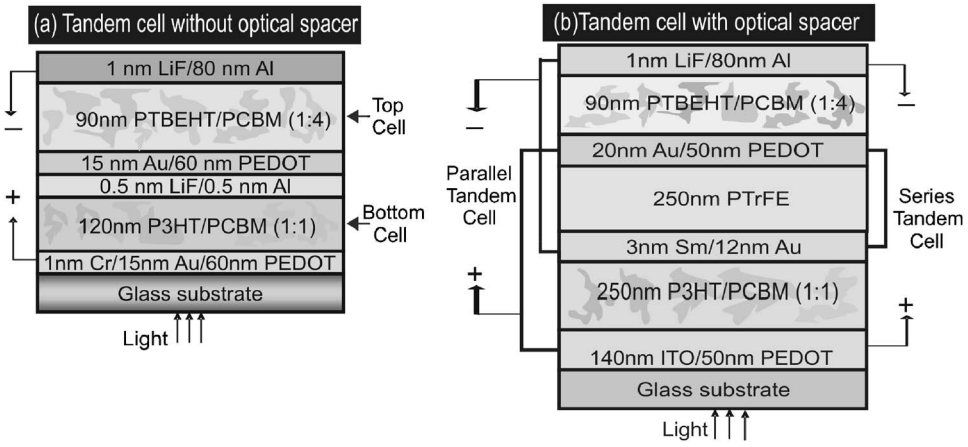

FIG. 1. (a) Schematic structure of the previously published tandem cell in which the bottom cell acts as an optical spacer. (b) Schematic structure of the second generation tandem cell in which an additional optical spacer is used that allows for independent tuning of the optical cavity. Two bulk heterojunction cells (bottom and top cells) are stacked in series or in parallel outside the device (four terminal devices). The absorption spectra of the two semiconducting polymers P3HT and PTBEHT are complementary.

Starck) was spin coated and dried in an oven at 140 °C for 15 min. The bottom cells were based on blends in a 1:1 ratio of regioregular P3HT (see inset Fig. 6) and the fullerene derivative[6,6]-phenyl C_{61} butyric acid methyl ester (PCBM) processed from chloroform. The P3HT:PCBM film was annealed at 135 °C for 2 h using a hot plate in the glove box under nitrogen atmosphere. The top cell was processed from a $CHCl_3$ solution of the poly(di-2-thienylthienopyrazine) derivative poly{5,7-di-2-thienyl-2,3-bis(3,5-di(2-ethylhexyloxy)phenyl) - thieno[3,4-b]pyrazine} (PTBEHT) (see inset Fig. 6) and PCBM in a 1:4 ratio. PTBEHT was synthesized from the corresponding dibrominated monomer via a condensation polymerization using bis(1,5-cyclooctadiene)nickel(0) [$Ni(COD)_2$].[24] PTBEHT was extensively purified by removing Ni with ethylenediamine tetraacetic acid (EDTA) disodium salt, Soxhlet extraction using different solvents, and finally a BioBeads gel permeation chromatography (GPC) column to remove the low molecular weight fraction. The molecular weights as determined with size exclusion chromatography are $M_n = 52\,000$ and $M_w = 160\,000$ [polydispersity index (PDI) = 3.1]. PTBEHT is soluble in most common organic solvents. The optical spacer was fabricated from poly(trifluoroethylene) (PTrFE) dissolved in methyl ethyl ketone (MEK).

All conjugated polymers and PCBM were dissolved in chloroform and mixed in the designated weight ratio. A proper spin program was chosen to tune the thicknesses of the layers (250 nm for P3HT:PCBM and 90 nm for PTBEHT:PCBM). For the cathode of the bottom cell, using a shadow mask, 3 nm samarium (Sm) and 12 nm Au were vapor deposited (at 10^{-7} mbar). PTrFE was dissolved in MEK and spin coated onto the bottom cell in various layer thicknesses. On top of the PTrFE layer, using shadow mask, 20 nm Au was evaporated and 50 nm PEDOT:PSS was spin coated. The complete stack was dried in a vacuum chamber at 10^{-2} mbar (1 Pa) for 30 min. For the active layer of the top cell, the polymer PTBEHT as electron donor and PCBM as acceptor were used in a 1:4 ratio. Both were dissolved in chloroform. A proper spin program was chosen to tune the thickness of the layers [90 nm PTBEHT:PCBM (1:4) film]. For the top contact, using a shadow mask, 1 nm LiF and 80 nm aluminum (Al) were thermally evaporated. The thicknesses of the different layers were measured by a Dektak 6M profilometer. All optical measurements were performed on a PerkinElmer Lamda 900 spectrometer. The *J-V* measurements (in dark and illuminated) were done by using Keithley 2400 source meter. The illumination was done using an AM1.5 simulated solar spectrum from a Steuernagel Solar-Constant 1200 light source with an intensity of $\sim 1000\ W/m^2$. The processing was done in a glove box under nitrogen and at room temperature.

III. RESULTS AND DISCUSSIONS

First the optical out coupling and then the electronic performance of the tandem cells are addressed. The materials and thickness of the electrodes are optimized to have a good optical transmission and a low in-plane resistance. Furthermore, the layer thicknesses of both subcells are optimized for their electronic transport. The bottom cell with the optical spacer processed on top is optimized for its optical transmission in order to harvest the maximum amount of photons on the (infra)red edge of the visible spectrum. Finally, all important parameters are used to design and optimize our tandem solar cell with an embedded optical spacer.

The two organic solar cells are linked together by an insulating, solution-processable, and transparent layer of PTrFE processed from a solution of MEK. This spin coated layer acts as an optical spacer. Due to the presence of the insulating layer of PTrFE the fabrication of the tandem cell now requires four electrodes. The electrodes of the bottom and the top cell can be connected externally in series or in parallel. Consequently, the contacts have to be highly conductive in order to extract and transport the charges from each subcell. Two of the four contacts used here in the tandem configuration are known to be efficient in BHJ solar cells, namely, 140 nm ITO/50 nm PEDOT:PSS as anode for the bottom cell and 1 nm LiF/80 nm Al as cathode of the top cell.[18–23] Now, the semitransparent cathode of the bottom cell and the semitransparent anode of the top cell have to be defined. The requirements for these electrodes are: as thin as possible to obtain maximum transparency, conductive enough to extract charge carriers, and stable during spin coating of the PTrFE optical spacer. For the cathode of the bottom cell 3 nm of Sm topped with 12 nm Au was found to be very transparent, highly conductive, and stable during spin coating of the PTrFE layer. The low work function of the Sm [~2.7 eV (Ref. 25)] provides an Ohmic contact with

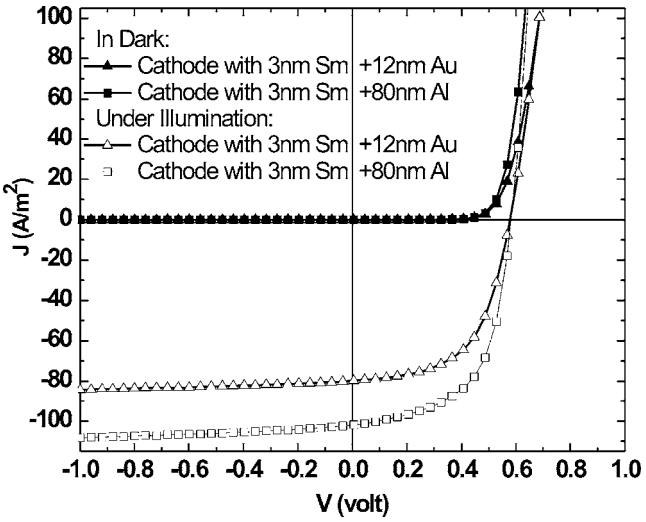

FIG. 2. Comparison between a semitransparent cathode made of 3 nm Sm/12 nm Au and a "perfect" mirror of 1 nm LiF/80 nm Al on top of the bottom cell consisting of a BHJ of 250 nm P3HT:PCBM (1:1). The fill factor and open-circuit voltage of both cells are the same but the photogenerated current of the cell with a semitransparent cathode is significantly lower.

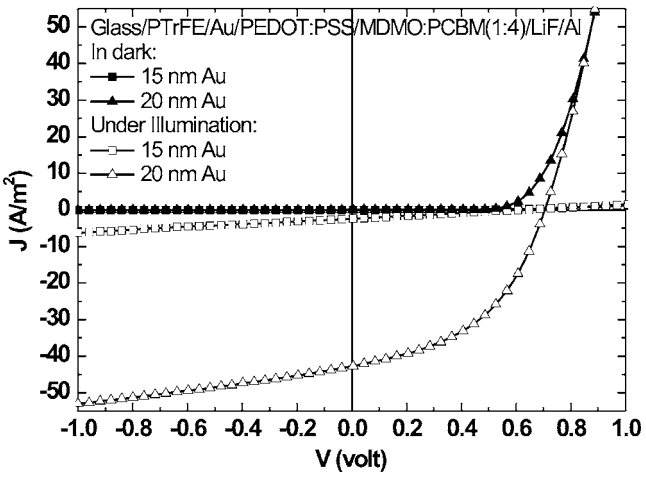

FIG. 3. Current density-voltage characteristics of a reference top cell structure with different gold thicknesses at the anode on 250 nm PTrFE are compared. On top of the gold layer a cell is processed based on 50 nm PEDOT:PSS/100 nm MDMO-PPV:PCBM (1:4)/1 nm LiF/80 nm Al. At a thickness of 15 nm the sheet resistance of the contact is too high which leads to a very poor performance of the cell.

the bottom cell in order to maximize the open-circuit voltage. The 12 nm Au layer has a sufficiently low resistance for transporting the charge carriers toward the external electrodes. Figure 2 demonstrates the difference between two BHJ single cells using ITO/PEDOT:PSS/250 nm P3HT:PCBM (1:1) with different cathodes. Both cells show the same FF (~64%) and V_{oc} (~0.6 V) but the cell with 3 nm Sm/12 nm Au cathode yields a lower photocurrent since this top electrode is semitransparent, resulting in a reduction of the amount of absorbed light. On the other hand, the reflection of a closed layer of 80 nm Al (perfect mirror) is ~100%, which results in a higher photocurrent for a solar cell topped with 80 nm Al.

On top of the PTrFE optical spacer a bilayer of 20 nm Au and 50 nm PEDOT:PSS was chosen for the anode of the top cell. The high and stable work function (~5.2 eV) of PEDOT:PSS forms an Ohmic contact for the top cell to extract the holes. In addition, PEDOT:PSS improves the wetting of the anode for the processing of the top cell. The 20 nm Au layer serves again as conducting layer to extract the holes. This Au layer needs to be optimized for its sheet resistance and optical transparency. To determine its optimal thickness (sheet resistivity versus optical transparency) a reference top cell is fabricated on top of a 250 nm thick layer of PTrFE. The reference top cell consists of x nm Au/50 nm PEDOT:PSS/100 nm MDMO-PPV:PCBM (1:4)/1 nm LiF/80 nm Al. As Fig. 3 demonstrates, at least 20 nm Au is needed to create a well-performing device. A thinner layer of Au (15 nm) leads to very high sheet resistance of the anode and, therefore, to a very poor performance of the cell. This is attributed to the surface roughness of the spin coated optical spacer of PTrFE, leading to the formation of a semicontinuous Au layer.

Now that we have optimized and defined all anodes and cathodes of our four terminal tandem solar cells, we can further optimize the layer thicknesses of the photoactive layers of the tandem solar cell. These layers can be independently optimized since the optical out coupling of the bottom cell can be tuned by the layer thickness of the PTrFE optical spacer (Figs. 1 and 7). Therefore, we have spin coated blends of P3HT:PCBM (1:1) with various layer thicknesses onto the substrates covered with 140 nm ITO/50 nm PEDOT:PSS and topped the devices off with 3 nm Sm/80 nm Al. The data in Fig. 4 demonstrate that a cell with a layer thickness of 250 nm of P3HT:PCBM (1:1) performs best. When the active layer is thinner (120 nm), the amount of absorbed photons is much lower and, consequently, a lower photocurrent is obtained. When the layer thickness is further increased to 450 nm, the amount of absorbed photons is only slightly increased, but the unbalanced transport of the charge carriers becomes a limitation; the buildup of space-charge results in a significant decrease of the fill factor, which in turn leads to lower total performance.[19]

For the top cell we used the conjugated polymer

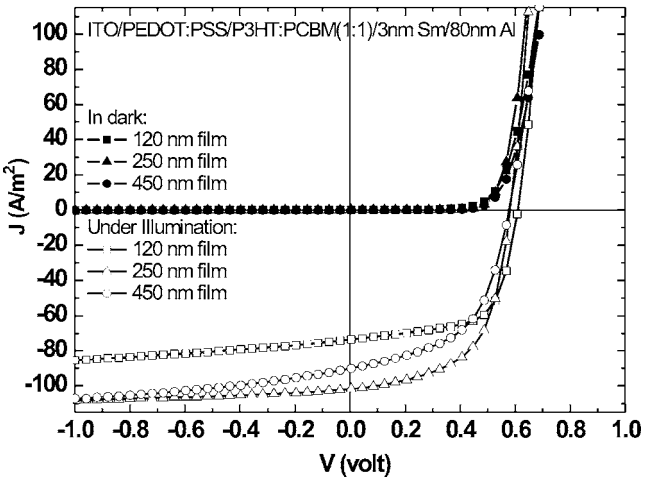

FIG. 4. Current-voltage characteristics of single BHJ bottom cells with various thicknesses of P3HT:PCBM (1:1). A layer thickness of 250 nm shows the best performance.

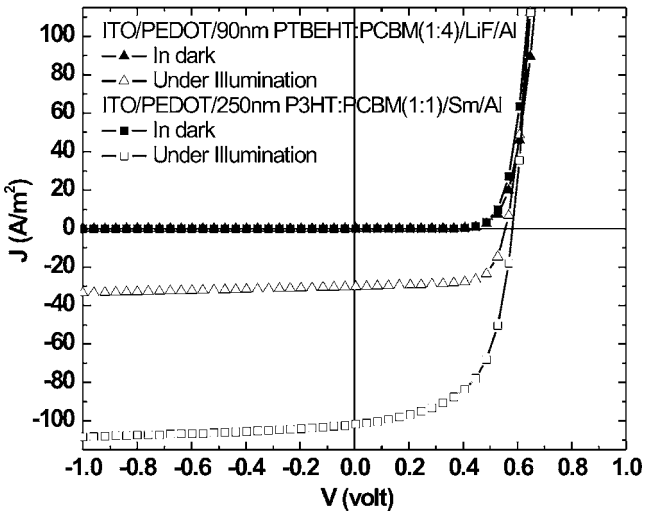

FIG. 5. The *J-V* characteristic of the active layers used in the bottom [250 nm P3HT:PCBM (1:1)] and top [90 nm PTBEHT:PCBM (1:4)] cells. These reference single cells are measured in dark and under illumination.

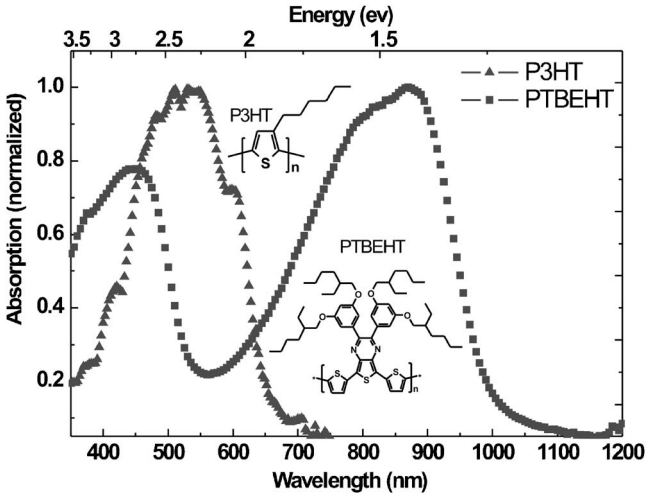

FIG. 6. Absorption spectra of the large band gap polymer P3HT and of the small band gap polymer PTBEHT with their maximum at 850 nm. The absorption spectra are complementary.

PTBEHT.[24] The thickness of the top cell made of PTBEHT:PCBM (1:4) is kept to 90 nm, which was found to give the best performance (chemical structure of PTBEHT is plotted in Fig. 6).[24,18] The *J-V* characteristics of the 250 nm P3HT:PCBM (1:1) and 90 nm PTBEHT:PCBM (1:1) solar cells are plotted in dark and under illumination ($\sim$1000 W/m^2, simulated AM1.5 solar spectrum) in Fig. 5.

The transparent layer of PTrFE is sandwiched between the semitransparent cathode of the bottom cell and the semitransparent anode of the top cell. This allows for the light transmitted through the bottom cell to interfere with the reflected light at the anode of the top cell. Therefore, the thickness of the PTrFE layer affects the total light output through the bottom stack before it reaches the top cell. After optimization of the layer thickness of the bottom cell, the wavelength of the transmitted light can now be tuned to match the absorption spectrum of the top cell by varying the thickness of the optical spacer (PTrFE layer). The combination of Sm and Au as the cathode for the bottom cell is inert for processing of the PTrFE optical spacer, which is spin coated from MEK. The advantage of choosing PTrFE is that it can be dissolved in a polar solvent such as MEK but not in solvents such as chloroform, chlorobenzene, or dichlorobenzene. As a result the solvents used for processing of the active layers of the bottom and the top cells (chloroform or chlorobenzene) are orthogonally compatible with the polar solvent (MEK) used for processing of the optical spacer. The layer thickness of this transparent PTrFE layer can be easily varied between several tens of nanometers and micrometers. To summarize, the processing steps are the following: ITO-coated glass substrates were covered with 50 nm PEDOT:PSS (anode of bottom cell). On top of the PEDOT:PSS anode a 250 nm P3HT:PCBM (1:1) blend is spin coated. The P3HT:PCBM film was annealed at 135 °C for 2 h using a hot plate in the glove box under nitrogen atmosphere. Then, 3 nm Sm and 12 nm Au (cathode of bottom cell) are evaporated, which are topped by spin coating the optical spacer (PTrFE from MEK). After evaporation of 20 nm Au onto the optical spacer, 50 nm PEDOT:PSS (anode of top cell) is spin coated and a solution of PTBEHT:PCBM (1:4) in chloroform is spin coated on top (90 nm). Finally, 1 nm LiF and 80 nm Al (cathode of top cell) were evaporated.

By using donor materials with nonoverlapping absorption spectra for the subcells in a tandem configuration, the utilization of two absorbing polymers with complementary absorption spectrum results in an enhanced photon harvesting of the solar spectrum.[18] Figure 6 depicts the normalized absorption spectra of the large band gap polymer P3HT and the small band gap polymer PTBEHT (Ref. 24) (see chemical structure of PTBEHT in inset of Fig. 6) that are used in this study.

We have performed optical measurements for various layer thicknesses of PTrFE to evaluate the optical transmission of the combined layers. Both the ITO/PEDOT:PSS/P3HT:PCBM/3 nm Sm/12 nm Au stack and the PTrFE sandwiched between 3 nm Sm/12 nm Au and 20 nm Au act as dielectric layers between semitransparent electrodes. As demonstrated in Fig. 7, the transmitted light through the bottom cell consisting of ITO/PEDOT:PSS/250 nm P3HT:PCBM/3 nm Sm/12 nm Au is not yet matched with the absorption spectrum of the top cell. Given the fact that the small band gap polymer (PTBEHT) absorbs between 700 and 950 nm, the optical cavity (or layer thickness) of the optical spacer has to be optimized in order to transmit in this wavelength range. Figure 7 demonstrates that a layer thickness of the optical spacer of 250 nm, in combination with 250 nm P3HT:PCBM/3 nm Sm/12 nm Au, results in an optical out coupling of the bottom stack that matches the absorption of the small band gap polymer in the top cell. The bottom cell processed from 250 nm P3HT:PCBM (1:1) topped with an optical spacer (PTrFE) of 250 nm transmits about 50% in the wavelength range that is absorbed by the small band gap polymer PTBEHT (Fig. 7, dotted line).

In this second generation tandem geometry, the bottom and the top cells can be electronically coupled either in series or in parallel. When the bottom and top cells are connected

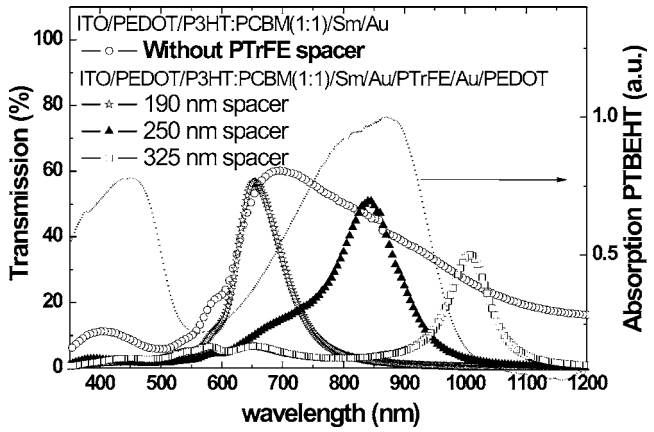

FIG. 7. Transmission of incident light through the bottom cell consisting of glass/140 nm ITO/50 nm PEDOT:PSS/250 nm P3HT:PCBM (1:1)/3 nm Sm/12 nm Au/x nm PTrFE/20 nm Au/PEDOT:PSS. For a blend of P3HT:PCBM (1:1) with a layer thickness of 250 nm (and no optical spacer), the light output is not yet matched with the absorption of the top cell (700–950 nm, spectrum given by the dotted line). By spin coating an additional transparent layer of PTrFE, the transmitted light can be tuned in order to match the absorption of the top cell.

in series, the open-circuit voltage (V_{OC}) of the tandem cell is equal to the sum of the open-circuit voltages of both individual cells. The photocurrent density of the tandem cell becomes limited by the lowest photocurrent density of the two subcells which is, in our tandem cell, the current of the top cell. As shown from the single reference cells (Fig. 5), the cells based on PTBEHT generate less photocurrent as compared to the P3HT based cells. Combined with the fact that the top cell is also illuminated with lower light intensity ($\sim$50%), the photocurrent of the top cell is substantially lower as compared to the bottom cell. The J-V measurements of the individual bottom and top cells and of the tandem cell connected in series are depicted in Fig. 8(a). As expected, the top cell strongly limits the photocurrent of the tandem cell.

In our four terminal tandem geometry, the two subcells can also be easily connected in parallel. Since both cells produce the same V_{OC} the tandem solar cell connected in parallel is expected to have the same V_{OC} as both subcells (no losses). In contrast, the current which can be extracted from the parallel tandem cell is now the sum of the photocurrents of the bottom and top cells. This implies that the tandem cell in parallel configuration is not limited by the lower current of the top cell. The current density-voltage characteristics for the bottom, top, and the parallel tandem cells are plotted in Fig. 8(b). Since the top cell generates a much lower photocurrent as compared to the bottom cell, the parallel tandem solar cell leads to a higher performance as compared to the tandem solar cell connected in series. Indeed, the open-circuit voltage of the parallel tandem cell is close to the V_{OC} of the bottom and top cells, while the current is the sum of both photocurrents generated by the two subcells. A direct comparison between the series and the parallel configuration is shown in Fig. 8(c); the series configuration has a high open-circuit voltage (V_{OC}=1.03 V), while the short-circuit current density (J_{SC}=16.3 A/m^2) is limited by the lower current of the top cell. The parallel configuration shows the same open-circuit voltage as both subcells

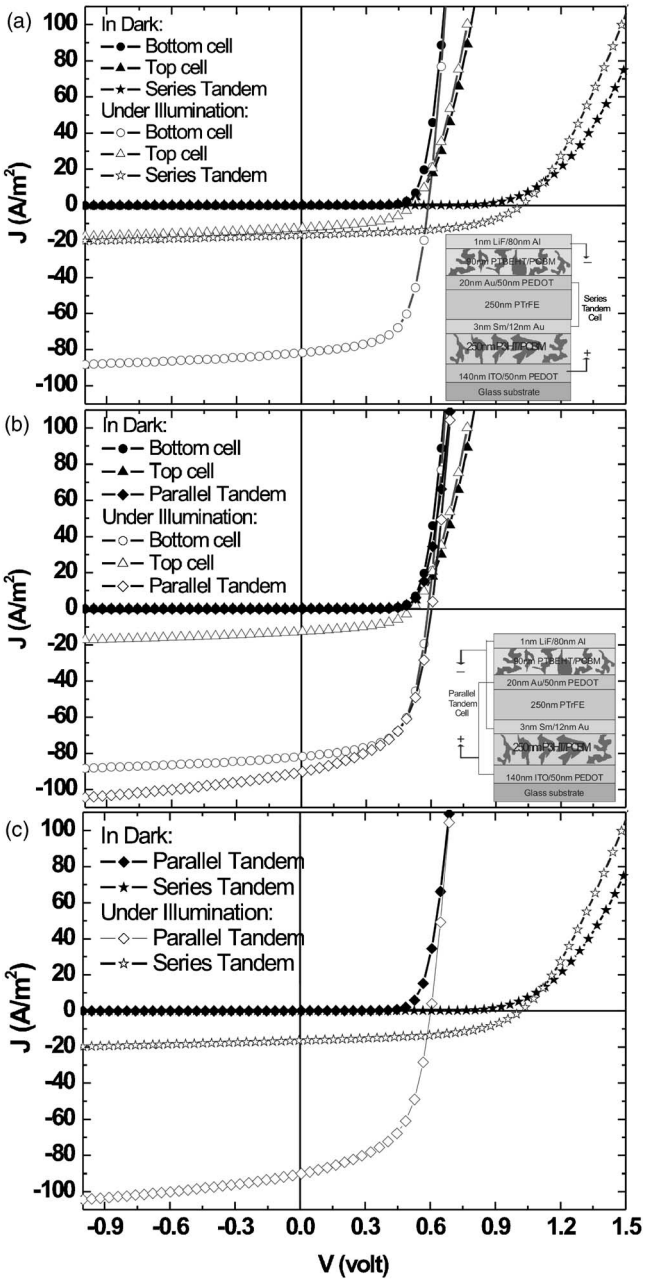

FIG. 8. (a) J-V characteristics of the bottom and top cells measured separately and the tandem cells connected in series in dark and under illumination. The current density is limited by the lowest current density of the two cells, and the open-circuit voltage is the sum of both subcells. (b) J-V characteristics of the bottom and top cells measured separately and the tandem cells connected in parallel in dark and under illumination. The current density is equal to the sum of both subcells, and the open-circuit voltage is limited to the lowest V_{OC} of the subcells. (c) The J-V characteristics of the series tandem cell vs the parallel tandem cell.

(V_{OC}=0.59 V), combined with a high short-circuit current density (J_{SC}=92.0 A/m^2). The values of the V_{OC}, J_{SC}, and FF of the bottom, top, series tandem, and parallel tandem solar cells are summarized in Table I. The performance of the parallel tandem cell is much better than the series tandem cell since the photocurrent of the tandem cell is limited by the low photocurrent of the top cell.[18] However, it should be noted that in the present parallel configuration, the performance hardly exceeds the performance of the bottom cell alone (estimated efficiency is 3% for both bottom and paral-

TABLE I. The quantitative values extracted from the *J-V* measurements of the individual and tandem photovoltaic cells.

Solar cell type	V_{OC} (V)	J_{SC} (A/m^2)	FF (%)
Bottom cell	0.60	81.6	64
Top cell	0.51	12.7	50
Series tandem cell	1.03	16.3	51
Parallel tandem cell	0.59	92.0	55

lel tandem cells). Since the current of this tandem cell is equal to the sum of the currents generated by both subcells, the lower FF of the top cell (50%) [compared to the high FF of the bottom cell (64%)] also affects the FF of the tandem cell (54%). This lower FF compensates the gain in photocurrent in the parallel tandem solar cell. In the case of two subcells having similar fill factors, the parallel configuration will always result in a tandem solar cell with higher performance as compared to the individual subcells.

IV. CONCLUSIONS

Solution-processed organic tandem solar cells were fabricated using an electrically insulating and solution-processable optical spacer. The optical spacers are based on the transparent poly(trifluoroethylene), which is dissolved in methyl ethyl ketone. This polar solvent is orthogonally compatible with the solvents of the active layers of the solar cells and leaves the bottom cell unaffected. By varying the thickness of the optical spacer, the transmission through the bottom cell and spacer is tuned to match the absorption of the top cell. This allows for an independent optimization of the thickness of the bottom cell for its best electrical performance. Furthermore, we can electrically address the tandem solar cells in series or in parallel. The performance of the series tandem solar cell is limited by the low current of the top cell, even though the V_{OC} is equal to the sum of both subcells and amounts to >1 V. The parallel tandem cell has a much higher efficiency since the V_{OC} of the parallel tandem cell is equal to the V_{OC} of both subcells and the photocurrent density is equal to the sum of the photocurrent densities of both subcells. The lower FF of the top cell limits the performance of the parallel tandem cell.

ACKNOWLEDGMENTS

Dr. Ronald C. G. Naber is acknowledged for fruitful discussions and assistance. Jan Harkema and Frans van der Horst are acknowledged for their technical assistance, and Floris B. Kooistra and Professor Jan C. Hummelen for providing PCBM. Professor Rene A. J. Janssen, Dr. Martijn M. Wienk, and Mathieu G. R. Turbiez of the Eindhoven University of Technology are acknowledged for the supply of the PTBEHT.

[1] S. Barth and H. Bässler, Phys. Rev. Lett. **79**, 4445 (1997).
[2] P. G. Dacosta and E. M. Conwell, Phys. Rev. B **48**, 1993 (1993).
[3] R. N. Marks, J. J. M. Halls, D. C. Bradley, R. H. Friend, and A. B. Holmes, J. Phys.: Condens. Matter **6**, 1379 (1994).
[4] J. J. M. Halls, C. A. Walsh, N. C. Greenham, E. A. Marseglia, R. H. Friend, S. C. Morahi, and A. B. Holmes, Nature (London) **376**, 498 (1995).
[5] G. Yu, J. Gao, J. C. Hummelen, F. Wudl, and A. J. Heeger, Science **270**, 1789 (1995).
[6] C. J. Brabec, N. S. Sariciftci, and J. C. Hummelen, Adv. Funct. Mater. **11**, 15 (2001).
[7] V. D. Mihailetchi, L. J. A. Koster, J. C. Hummelen, and P. W. M. Blom, Phys. Rev. Lett. **93**, 216601 (2004).
[8] C. L. Braun, J. Chem. Phys. **80**, 4157 (1984).
[9] K. M. Coakley and M. D. McGehee, Chem. Mater. **16**, 4533 (2004).
[10] D. W. Sievers, V. Shrotriya, and Y. Yang, J. Appl. Phys. **100**, 114509 (2006).
[11] M. Hiramoto, M. Suezaki, and M. Yokoyama, Chem. Lett. **1990**, 327.
[12] P. Peumans, V. Bulovic, and S. R. Forrest, Appl. Phys. Lett. **76**, 2650 (2000).
[13] J. Xue, S. Uchida, B. P. Rand, and S. R. Forrest, Appl. Phys. Lett. **85**, 5757 (2004).
[14] P. Peumans and S. R. Forrest, Appl. Phys. Lett. **79**, 126 (2001).
[15] A. Yakimov and S. R. Forrest, Appl. Phys. Lett. **80**, 1667 (2002).
[16] J. Drechsel, B. Männig, F. Kozlowski, M. Pfeiffer, K. Leo, and H. Hoppe, Appl. Phys. Lett. **86**, 244102 (2005).
[17] K. Triyana, T. Yasuda, K. Fujita, and T. Tsutsui, Jpn. J. Appl. Phys., Part 1 **43**, 2353 (2004); Thin Solid Films **477**, 198 (2005).
[18] A. Hadipour, B. de Boer, J. Wildeman, F. B. Kooistra, J. C. Hummelen, M. G. R. Turbiez, M. M. Wienk, R. A. J. Janssen, and P. W. M. Blom, Adv. Funct. Mater. **16**, 1897 (2006).
[19] M. Lenes, L. J. A. Koster, V. D. Mihailetchi, and P. W. M. Blom, Appl. Phys. Lett. **88**, 243502 (2006).
[20] L. J. A. Koster, V. D. Mihailetchi, R. Ramaker, and P. W. M. Blom, Appl. Phys. Lett. **86**, 123509 (2005).
[21] L. J. A. Koster, V. D. Mihailetchi, H. Xie, and P. W. M. Blom, Appl. Phys. Lett. **87**, 203502 (2005).
[22] V. D. Mihailetchi, H. Xie, B. de Boer, L. J. A. Koster, and P. W. M. Blom, Adv. Funct. Mater. **16**, 699 (2006).
[23] V. D. Mihailetchi, H. Xie, B. de Boer, L. M. Popescu, J. C. Hummelen, P. W. M. Blom, and L. J. A. Koster, Appl. Phys. Lett. **89**, 012107 (2006).
[24] M. M. Wienk, M. G. R. Turbiez, M. P. Struijk, M. Fonrodona, and R. A. J. Janssen, Appl. Phys. Lett. **88**, 153511 (2006).
[25] *Handbook of Chemistry and Physics*, 75th ed., edited by D. R. Lide (CRC, Cleveland/Boca Raton, 1995); we have evaporated 20 nm samarium on glass and measured its work function to be 2.4 eV with the Kelvin probe under N_2 atmosphere.